minerals

MDPI

Article

Petrographic and Geochemical Inferences for Genesis of *Terra Rossa*: A Case Study from the Apulian Karst (Southern Italy)

Francesca Micheletti [1,*], Annamaria Fornelli [1], Luigi Spalluto [1], Mario Parise [1], Salvatore Gallicchio [1], Fabrizio Tursi [2] and Vincenzo Festa [1]

[1] Earth and Geo-Environmental Sciences Department, Aldo Moro University of Bari, 70125 Bari, Italy
[2] Earth Sciences Department, University of Turin, 10125 Turin, Italy
* Correspondence: francesca.micheletti@uniba.it; Tel.: +39-080-5442609

Abstract: *Terra rossa* is a reddish clay soil which is often present on the surface of limestone in regions with a Mediterranean-type climate. Its genesis is a controversial subject in terms of the origin of the parent material, from the residuum of underlying (carbonate/dolomite) bedrock in the absence/presence of an external silicate contribution (e.g., aeolian dust). Within this context the main goal of the present work was the understanding of the geochemical processes leading to the formation of the *terra rossa* starting from the carbonate bedrock. We report the results of a multi-method analysis on a *terra rossa* deposit occupying the bottom of a Quaternary karst depression on Mesozoic limestones exposed in the Murge area (Apulia Foreland, southern Italy). Geological, petrographic, textural, and chemical data were collected on karst products (reddish calcite incrustations and nodules, and fine-grained portion of *terra rossa*) by a detailed field mapping, optical microscopy, XRF and fusion ICP/MS analyses and by scanning electron microscope. New collected data show that the mineralogical composition of reddish incrustations and nodules is comparable, consisting of fibrous and impure calcite, detrital fragments of quartz, K-feldspar, zircon and authigenic minerals as (Mn, Ba, Ca) phases, (Al, Si, Mn, Fe, Mg, Ba, Ca) minerals, Fe-kaolinite and anatase. The prevailing minerals, instead, in the fine-grained portion of *terra rossa* are hematite, kaolinite, and goethite. Based on the chemical composition, and especially on REE patterns, a progressive interaction of silicate aqueous solutions (with Al, Si, Fe), containing pelite material, with the calcareous bedrock, as a source of carbonic acid, was the process driving the formation of *terra rossa*. Obtained results add new elements to the definition of the long-lasting question about the genetic processes responsible for the formation of *terra rossa*, corroborating their polygenetic origin, as result of limestone alteration in conjunction with the chemical interaction with allochthonous siliciclastic material.

Keywords: *terra rossa*; karst limestone; residual deposits; silicate input; southern Italy

Citation: Micheletti, F.; Fornelli, A.; Spalluto, L.; Parise, M.; Gallicchio, S.; Tursi, F.; Festa, V. Petrographic and Geochemical Inferences for Genesis of *Terra Rossa*: A Case Study from the Apulian Karst (Southern Italy). *Minerals* **2023**, *13*, 499. https://doi.org/10.3390/min13040499

Academic Editor: Santanu Banerjee

Received: 1 March 2023
Revised: 29 March 2023
Accepted: 29 March 2023
Published: 31 March 2023

1. Introduction

Terra rossa is a reddish clayey to silty-clay material, which covers limestones and dolostones in the form of a discontinuous layer ranging in thickness from a few centimeters to several meters. Thick accumulations of *terra rossa* characterize the epikarst [1,2], that is the outer portion of karst terrains, with a strong effect on the recharging of karst aquifers [3–5]. Several authors considered the *terra rossa* as a polygenetic relict soil formed during the Tertiary and/or hot and humid periods of the Quaternary [6,7]. In karst terrains not affected by terrigenous sediment supply, *terra rossa* may have formed exclusively from the insoluble residue of carbonates [8,9]. However, in several cases *terra rossa* would appear to be genetically linked to a variety of parent materials including aeolian dust, volcanic material and/or terrigenous clastic inputs that triggered reaction processes in the underlying carbonate terrains [6,7,10].

One of the best places to investigate the debated origin of *terra rossa* is the Apulian Foreland (Figure 1a), characterized by widespread cropping out of Mesozoic inner shelf

carbonates of the Apulia Platform domain along with residual deposits related to multiple exposure phases [11,12]. Turonian *terra rossa* rich in bauxite [13–18] and clay-rich thin beds within Cretaceous limestones [19], are geochemically and mineralogically well constrained in the Apulian Foreland. Authors in [13–18], based on a large amount of data, supposed that the source material of the Turonian bauxite deposits cropping out in the Apulian Foreland consists of a combination of magmatic (distant windborne volcanic/plutonic particles) and siliciclastic (of cratonic origin) inputs mixed with degradation products of limestones. A binary mixing model with a combined contribution of carbonate residuum and windborne dust (e.g., pyroclastic material) was invoked by [19] for the clayey interlayers within Cenomanian–Coniacian limestones cropping out in the Apulian Foreland.

However, although mineralogical and geochemical analyses have been carried out on the post-Cretaceous residual deposits from the Apulian Foreland [20,21], the related *terra rossa* need to be better constrained in terms of genesis and parent material. Through the examination of the residuum of the carbonate rocks after karst dissolution, research in [20] attributes the observed silica in *terra rossa* to external marine source. Apulian red soils are similar, in terms of chemical, physical and mineralogical properties, to the previously studied *terra rossa* from Morocco, Greece and Spain, and, notably, to those from Sardinia (central Italy) and Istria (Croatia) [21]; their mineralogical and geochemical features suggested that both allochthonous and autochthonous materials contributed to the formation of the *terra rossa* in the Apulia Foreland.

In an attempt to acquire a better knowledge of the genetic processes and parent materials of the *terra rossa*, the so-called *Vuotano Santiquando*, a karst depression extending for 3000 m^2 formed during the late Quaternary phase of the Murge emersion on Cretaceous limestones, has been selected as a study area (Figure 1b,c). This site falls in the Alta Murgia National Park (Geosite n. CGP0043) and has a great naturalistic interest, hosting a temporary Mediterranean pond [22,23]. The main goal of the present paper is the understanding of the geochemical processes leading to the formation of *terra rossa* as a possible result of the pure limestone alteration and/or of the chemical interaction with external siliciclastic materials, which may have partially covered the underlying carbonate rocks. To this aim, a multi-method analysis was performed by geological mapping, petrography, XRF and fusion ICP/MS analyses, and use of scanning electron microscopy.

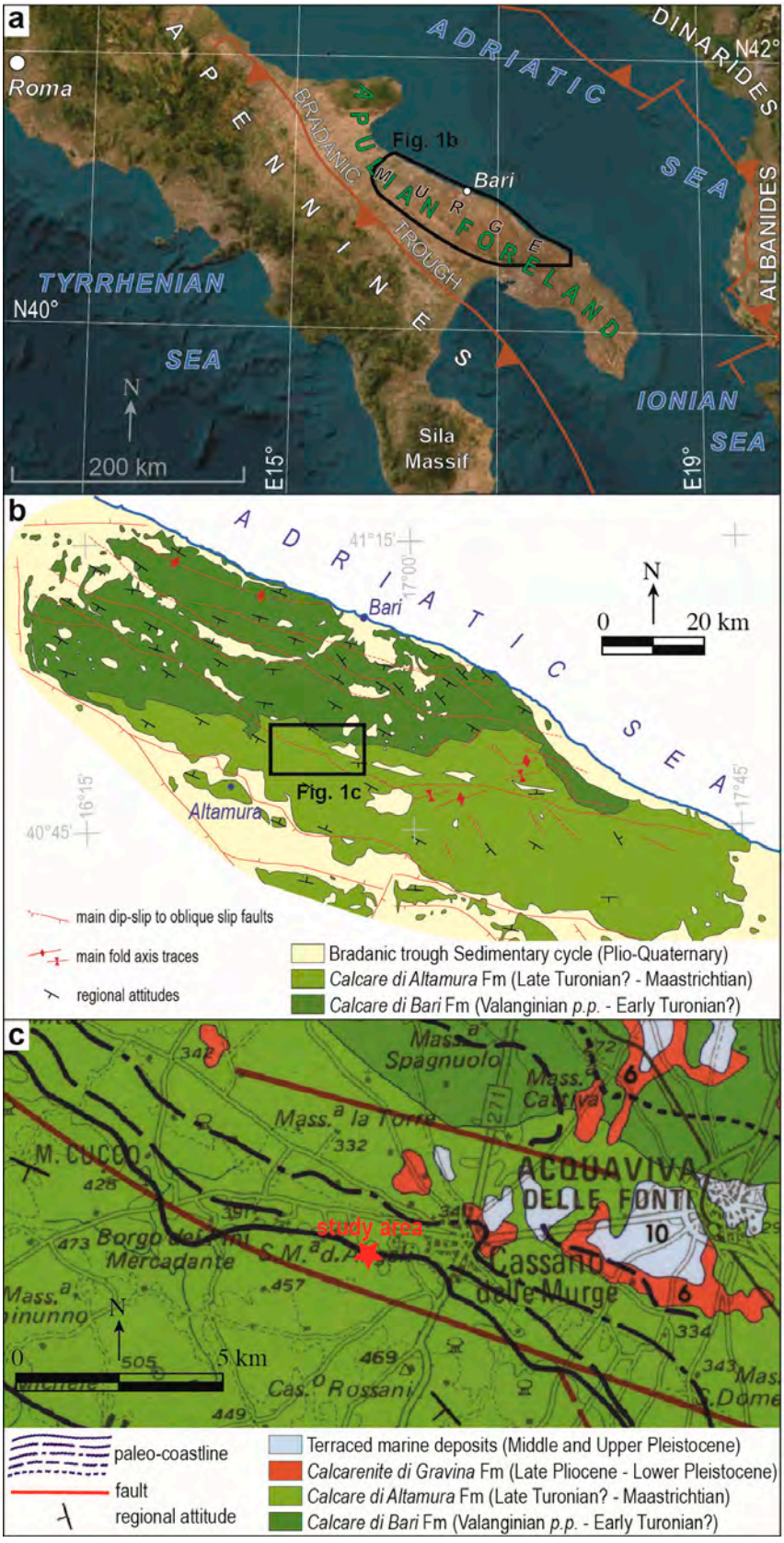

Figure 1. (**a**) Schematic structural map of the region around the Apulian Foreland (simplified after [24]); the thick closed line encloses the area in (**b**); (**b**) Geological and structural sketch map of Murge (modified after [11,25,26]); the rectangle with thick perimeter encloses the area in (**c**); (**c**) Geological map including the study area (i.e., the filled red star) (modified after [11]).

2. Geological Setting

The Apulian Foreland represents the Plio–Pleistocene foreland of both the Dinarides–Albanides–Hellenides and the Apennines orogens [27,28] (Figure 1a). Middle Jurassic–Upper Cretaceous inner platform carbonates of the Apulia Platform realm diffusely crop out in the Apulian Foreland, where they have a thickness of ca. 4 km [11,12,28].

In the Murge area, i.e., the central sector of the Apulian Foreland, the limestones and dolostones belong to the widely exposed *Calcare di Bari* Fm (Valanginian p.p.–Early Turonian?), stratigraphically overlaid by the *Calcare di Altamura* Fm (Late Turonian–Maastrichtian) [11,12] (Figure 1b). These two formations are in contact through an unconformity marked locally (especially to the west, in the Murge area) by the presence of Turonian bauxites (Figure 1b), related to a prolonged (about 4 myrs long) exposure phase of the Apulia Carbonate Platform (e.g., [11,28]).

A subsequent long exposure phase of the Apulia Platform occurred in the Murge during Tertiary, testified by development of karst processes [29,30] and presence of *terra rossa* levels in places buried by Plio–Pleistocene transgressive marine calcarenites, i.e., the *Calcarenite di Gravina* Fm, at the base of the Bradanic trough sedimentary cycle [31] (Figure 1b). Finally, the late Quaternary phase of emersion of Murge, with the sea retreat up to the present-day Adriatic Sea coastline (Figure 1b), was characterized by the sedimentation of mixed carbonate and siliciclastic terraced marine deposits [11,28,32], as well as by the further development of karst phenomena on the Cretaceous carbonate bedrock [30,33,34]. Remnants of the *Calcarenite di Gravina* Fm and of the terraced marine deposits disconformably overlay the Cretaceous carbonates in the area around the studied morphological depression (Figure 1c) (e.g., [11,32]).

3. Material and Methods

To achieve the main goal of this paper, a detailed geological mapping has been firstly carried out in the area around the morphological depression characterized by the presence of *terra rossa* (Figure 2a–c). Sampling was conducted from both the carbonate bedrock (e.g., Figure 2d) and the related karst products cropping out in the area (Figures 2e–g and 3).

Textural-petrographic analysis was performed, using polarized optical microscope, on thin sections obtained from many samples of the studied deposits.

SEM-EDS analyses (micro-textural features and semiquantitative mineral chemistry) were performed with a LEO-EVO50XVP (Carl Zeiss AG, Oberkochen, Baden-Württemberg, Germany) coupled with an X-max (80 mm^2) Silicon drift Oxford detector equipped with a Super Atmosphere Thin Window©. Semi-quantitative analyses were obtained using the following operating conditions: 15 kV accelerating potential, 500 pA probe current, about 25 kcps as output count rate on the whole spectrum, counting time 50 s and 8.5 mm working distance. The samples observed by SEM were the red incrustations and the red calcite nodules.

Major element analyses were carried out on fifteen samples: unaltered limestones (n = 2), red incrustation (n = 2), red calcite nodules (n = 8) and a fine-grained portion of *terra rossa* (n = 3). The analyses were performed by wavelength dispersive X-ray fluorescence spectroscopy (WD-XRF) from Panalytical (AXIOS-Advanced apparatus) (Malvern Panalytical, Great Malvern, UK) (equipped with a rhodium super sharp end-window X-ray tube at the Earth and Geo-environmental Sciences Dept. (Aldo Moro University of Bari, Italy). Analytical operating conditions were an X-ray tube set at 60 kV and 66 mA; LiF 220 diffracting crystal; and scintillator detector for X-rays collection. The intensity ratios of some trace elements such as Rb, Sr, Y, Zr and Nb were measured as proposed in [35].

Some trace element analyses including rare earth elements (REE) were performed on six samples (red incrustation, n = 1; red calcite nodules, n = 2; fine-grained portion of *terra rossa*, n = 3) by fusion ICP/MS at Actlabs® laboratories, in Ancaster, Hamilton, ON, Canada.

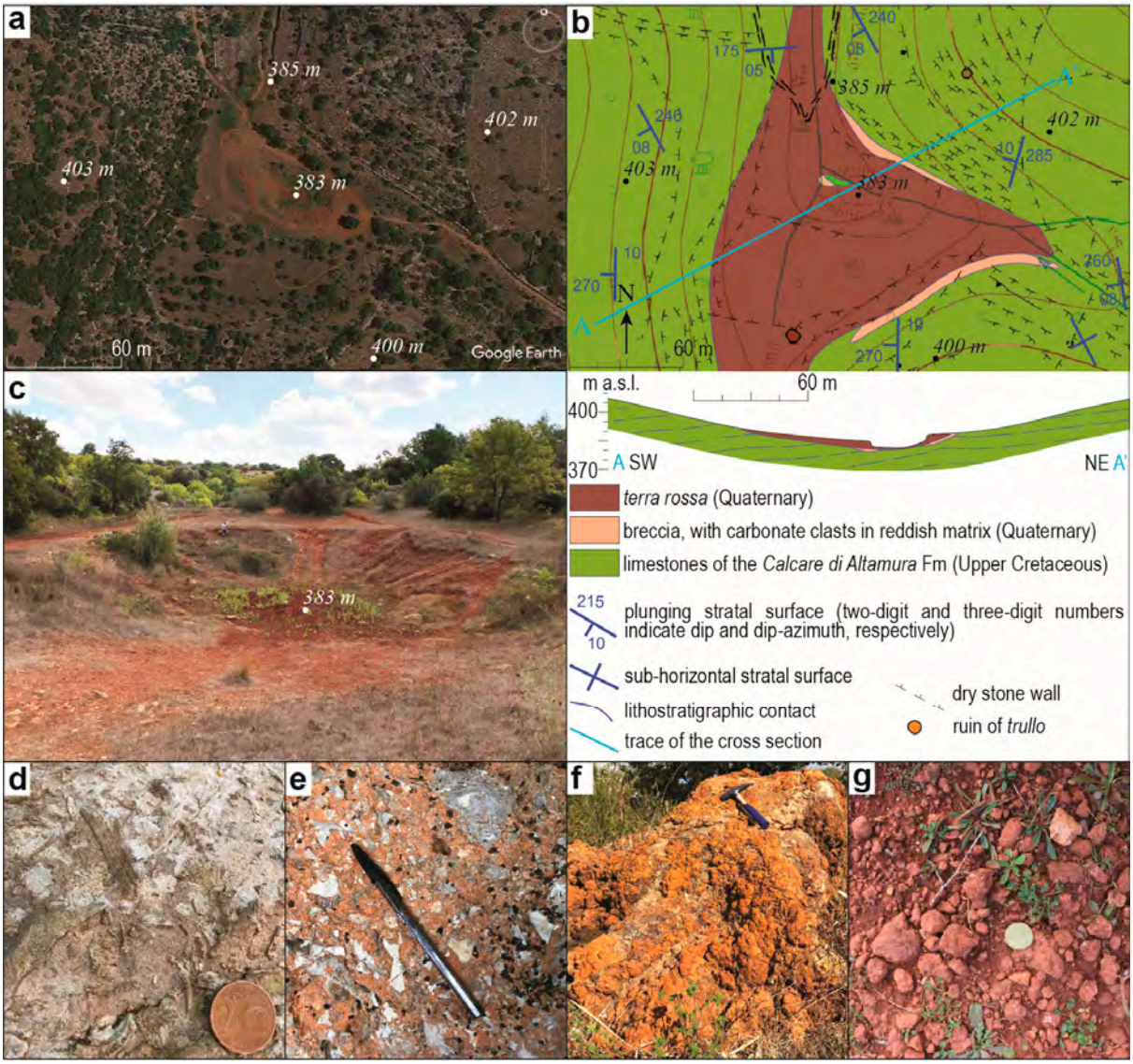

Figure 2. (**a**) Satellite image of the study area (Figure 1c for location); the geographic coordinates of the minimum elevation (383 m a.s.l.), at the bottom of the morphologic depression, are 40°53′02.70″ N, 16°44′48.88″ E; (**b**) Geological map of the study area and cross-section; (**c**) View of the small basin within the *terra rossa*, at the bottom of the morphological depression; (**d**) Detail of a wackestone rich in rudist fragments of the *Calcare di Altamura* Fm; (**e**) Detail of the breccia, with carbonate clasts in a reddish matrix; (**f**) Detail of the incrustations on a limestone block; (**g**) Reddish nodules in the fine-grained *terra rossa*.

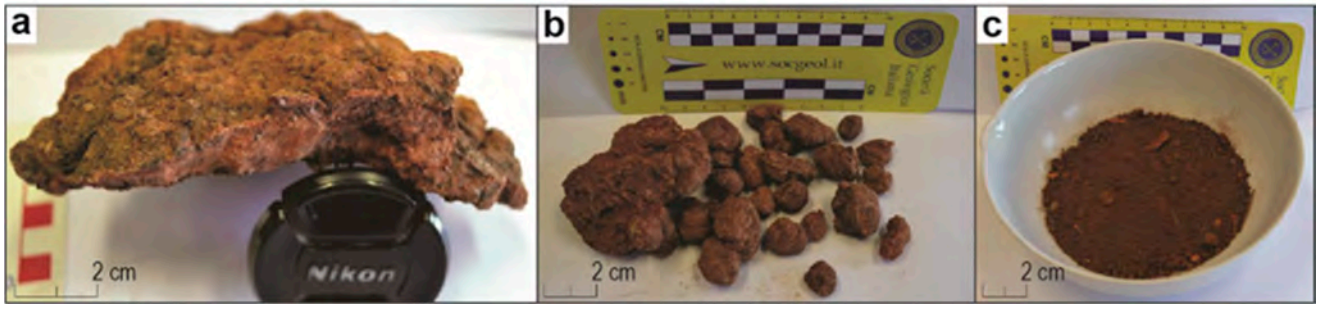

Figure 3. (**a**) Sample of calcite incrustation (see also Figure 2e); (**b**,**c**) Samples of red calcite nodules and fine-grained material, respectively (see also Figure 2f), in the *terra rossa*.

4. Results

4.1. Field Observations and Sampling

The study area is represented by a morphologic depression, i.e., a generic doline, located at the junction of two relatively small dry open V-shaped valleys (Figure 2a,b), collecting the surface runoff from the surrounding catchment and acting as an endorheic basin. In our case study, the *terra rossa* occurs in a sub-planar area of about 3000 m^2 (Figure 2a,b); a further smaller depression, up to 3 m deep and with a diameter of about 20 m, opens within the *terra rossa* (Figure 2c), at the bottom of the doline. This small basin may be of anthropogenic origin, due to the removal of *terra rossa*. The gentle slopes surrounding the sub-planar area reach an elevation around 400 m a.s.l. roughly at 100 m from the center of the small basin (Figure 2a,b), the latter at an elevation of 383 m a.s.l. (Figure 2a–c). The doline developed in the carbonate succession of the *Calcare di Altamura* Fm, whose stratal surfaces generally show gentle dips, up to 10°, and variable dip-directions from south to west (Figure 2b).

The *Calcare di Altamura* Fm, cropping out with a thickness of about 30 m (Figure 2b), shows the typical limestone lithotypes, i.e., well-stratified mudstones, wackestones and packstones rich in rudists, and is whitish and/or light brownish in color (Figure 2d). At the contact with the *terra rossa*, the *Calcare di Altamura* Fm is in places covered by a breccia, from matrix- to clast-supported, composed of carbonate clasts in a well-cemented reddish matrix (Figure 2e); the breccia crops out in patches, up to a couple of meters thick, in the western side of the morphologic depression (Figure 2b). Furthermore, the limestones are widely affected by brownish/yellowish humped to nodular incrustations, up to 4 cm thick (Figure 2f). Reddish nodules, with a diameter up to 4 cm, coalescing as well, are mixed with reddish fine-grained material giving rise to the *terra rossa* (Figure 2g), the latter reaching a maximum thickness of 5 m.

Samples were collected from the *Calcare di Altamura* Fm limestones and the related karst products, i.e., the incrustations (Figure 3a), and the nodules (Figure 3b) together with the fine-grained material (Figure 3c) of *terra rossa*.

4.2. Textural-Petrographic Analysis

4.2.1. Unaltered Limestones

Unaltered limestones (Figure 2d) consist of wackestones and packstones made up of bioclastic fragments, with a prevalence of rudists, benthic foraminifers, ostracodes and calcareous algae (Figure 4a).

The main recognized taxa are: *Accordiella conica*, *Dyciclina schlumbergeri*, *Scandonea samnitica*, *Moncharmontia appenninica*, and miliolids (benthic foraminifers); *Thaumatoporella parvovesiculifera* and *Aeolisaccus kotori* (algae). The facies association has been interpreted as indicative of shallow-water carbonate deposits corresponding to protected lagoons developed in the inner part of the Apulia Platform [36,37]. The benthic foraminifera association belonging to the *Rotorbinella scarsellai* and *Accordiella conica* Zone [38], indicates the Coniacian–Early Campanian time interval [39]. Based on facies association and stratigraphic features, the bedrocks of the studied *terra rossa* can be referred to the lower part of the *Calcare di Altamura* Fm succession cropping out in the Murge area.

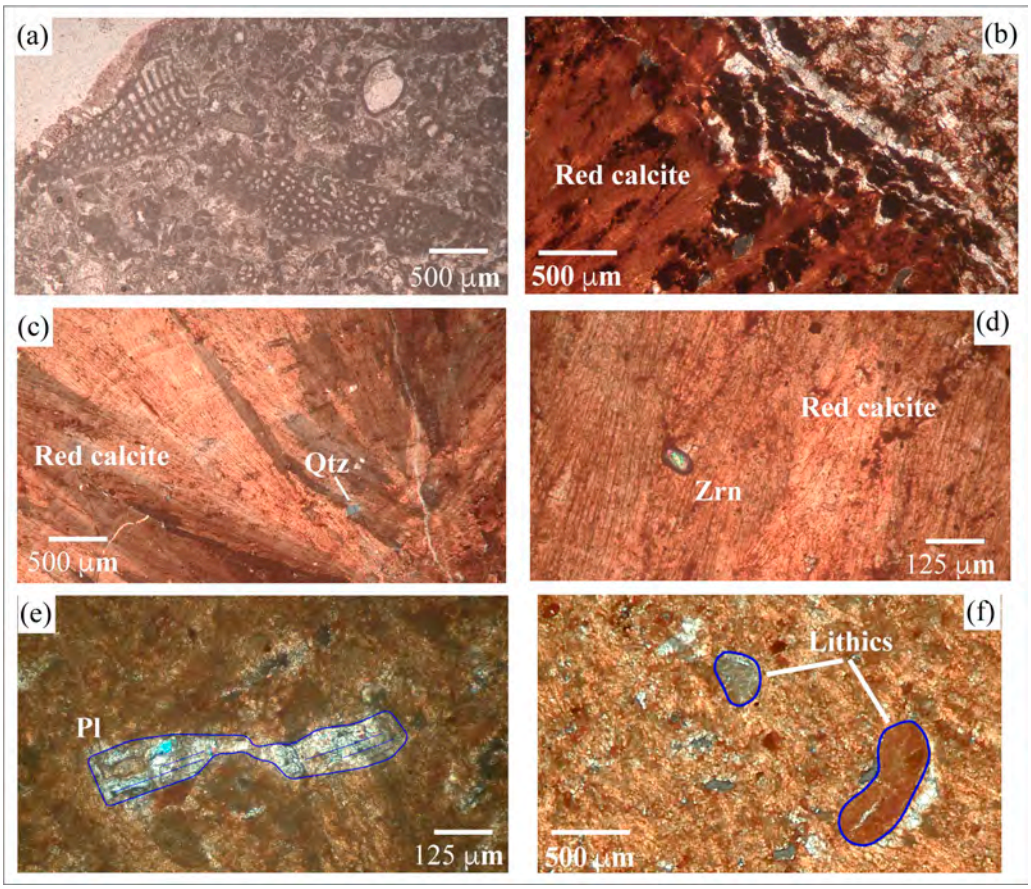

Figure 4. Microphotographs of studied samples: (**a**) Bioclastic packstone made up of abundant coated benthic foraminifers (CA4 sample, plane polarized light); (**b**) Gradual transition from intact limestone to weathered one, fading to the red calcite incrustation (CA2C sample, proceeding from NE to SW in the photo, plane polarized light); among red columnar calcite fibers in nodules are recognizable: (**c**) Monocrystalline quartz clasts (BA5L sample, crossed polarized light), (**d**) Zircon crystal (BA5L sample, crossed polarized light), (**e**) Partially preserved plagioclase crystal in which the typical polysynthetic twinning is detectable (BA5A sample, crossed polarized light); (**f**) Strongly altered polymineralic lithic fragments with a ghost porphyritic texture (BA5 sample, plane polarized light).

4.2.2. Karst Products

Upwards, the intact limestone (bedrock) gradually becomes more fractured and altered, up to red calcite incrustation with thickness varying from a few millimeters to 0.5–3.0 cm (Figures 2f and 3a). The red calcite incrustations begin to develop on the bedrock by elongated fibers up to columnar, growing perpendicular to the substrate (Figure 4b).

Among the fibrous calcite, some silicate phases such as monomineralic angular clasts of quartz and feldspar, and zircon crystals occur, together with opaques. Under the scanning electron microscope, several small inclusions of authigenic minerals can be observed (Figure 5a). From pure calcite forming the bedrock, a red impure calcite containing Al, Si and Fe developed as fibers (Figure 5b). Among the impure calcite, well-formed phases containing Si, Al, and Fe, probably Fe-kaolinite, seem to be developing (Figure 5b). The most evident minerals consist of (Mn, Ca, Ba) phases, present as a corona distant about 4 mm from unaltered limestone. Some portions of these luminescent grains show enrichment of Si, Al, and Fe (Figure 5b). The Mn-phases represent typical levels in the red incrustations forming the support of re-growth of red fibrous calcite.

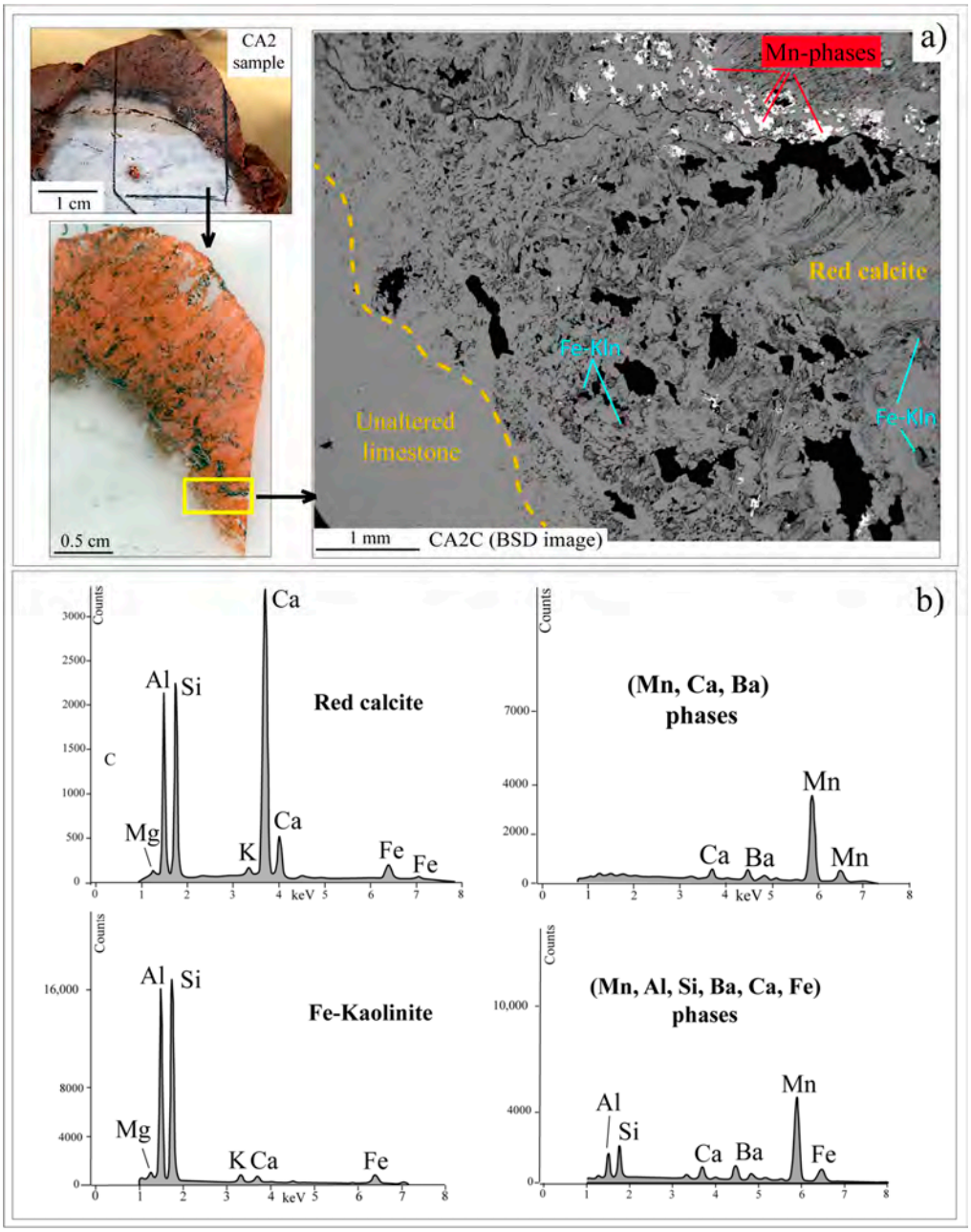

Figure 5. (**a**) Macroscopic image of red incrustation and relative thin section; on the right, a BSD-SEM image; (**b**) Qualitative analyses of some mineral phases in the red incrustation.

The centimetric nodules are essentially made up of red calcite with radial growth (Figures 3b and 4c). Small angular grains of quartz and feldspar are interspersed among calcite fibers; locally, zircon crystals and some lithic fragments in which a ghost porphyritic texture can be glimpsed (Figure 4c–f), are widespread between them.

Some typical nodules were observed under SEM. The structure of red nodules is radial, formed by impure red calcite fibers, containing Al, Si and Fe, radiating from the core. Among columnar fibrous calcite, detrital minerals such as quartz, K-Feldspars and zircons are interspersed together with new authigenic phases as anatase, Fe-kaolinite and (Mn, Ba, Ca) phases having spongy or homogeneous textures (Figure 6). The peripheral area of a calcite nodule (BA5 sample) contains a lithic fragment in which (Mn, Ba, Ca) or (Mn, Al, Si, Ba, Ca, Fe) phases, such as those present in the red incrustations, are present. In this lithic fragment further silicate phases such as quartz, K-feldspar and illite are interspersed (Figure 6).

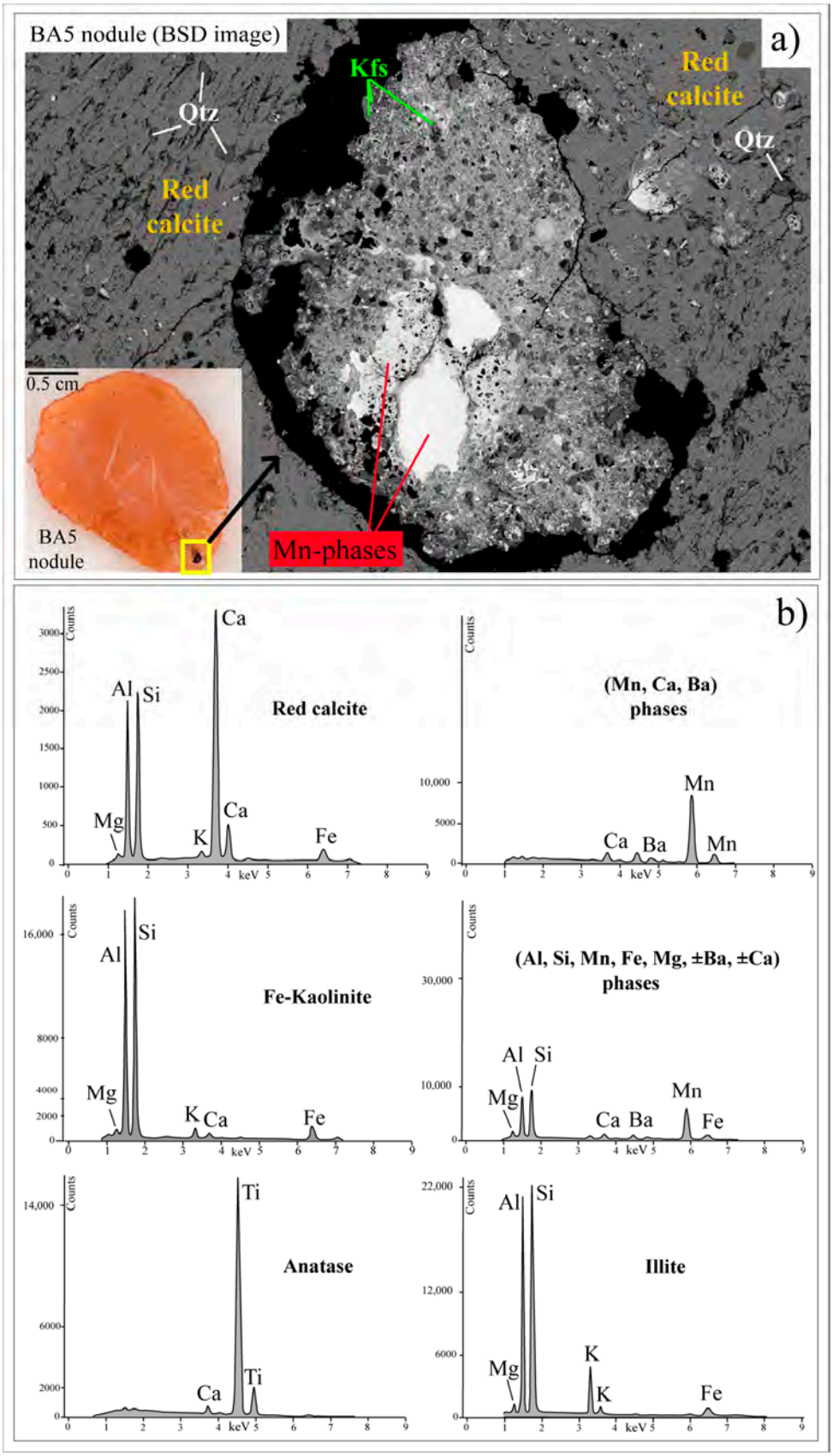

Figure 6. (**a**) Red calcite nodule BA5 and the detail of a lithic fragment incorporated in its peripheral portion (BSD-SEM image); (**b**) SEM-ED spectra relative to the several phases revealed in the lithic fragment and nodule.

A qualitative analysis of the mineral phases in a lithic fragment with ghost porphyritic texture (Figure 4f, smaller grain almost in the center of the image) shows some grains of K-feldspar, quartz, and Fe-oxide on which impure calcite is scattered.

Concerning the fine-grained *terra rossa*, first qualitative XRD analyses show the prevalent presence of goethite, kaolinite, and hematite as new mineral phases. Moreover, observations under stereo microscopy reveal the presence of a wide spectrum of silicate minerals, such as quartz, feldspar, micas, polymineralic aggregates, opaques, and zircons.

4.3. Geochemistry

Chemical analyses were performed on selected samples (Table 1) of unaltered limestones (n = 2), red incrustations (n = 2), calcite nodules (n = 8), and the fine-grained portion of *terra rossa* (n = 3).

Table 1. Major and trace element composition of the studied samples (XRF method).

	Sample	SiO_2	TiO_2	Al_2O_3	Fe_2O_3	MnO	MgO	CaO	Na_2O	K_2O	P_2O_5	LOI	Rb	Sr	Y	Zr	Nb
Limestone (bedrock)	CA1	0.14	0.00	0.08	0.02	0.03	0.13	56.57	0.02	0.00	0.00	43.00	6	172	1	7	1
Limestone (bedrock)	CA2	0.12	0.00	0.07	0.03	0.04	0.12	56.33	0.02	0.00	0.00	43.26	5	125	3	6	1
	mean	**0.13**	**0.00**	**0.08**	**0.03**	**0.04**	**0.13**	**56.45**	**0.02**	**0.00**	**0.00**	**43.13**	**6**	**149**	**2**	**7**	**1**
Cal incrustation (0.5 cm)	CA1C	1.36	0.03	0.76	0.27	0.04	0.16	54.81	0.02	0.06	0.00	42.49	10	163	14	17	2
Cal incrustation (2 cm)	CA2C	6.52	0.15	4.46	1.79	0.90	0.19	47.64	0.03	0.24	0.00	38.09	26	26	66	39	5
Cal nodule	BA1	9.09	0.26	4.14	1.70	0.02	0.18	47.26	0.03	0.29	0.00	37.02	28	22	50	70	7
Cal nodule	BA2	9.12	0.27	4.25	1.87	0.11	0.19	47.24	0.04	0.33	0.00	36.58	30	24	62	87	7
Cal nodule	BA3	8.19	0.25	3.88	1.85	0.03	0.18	48.27	0.03	0.29	0.00	37.02	31	25	62	83	7
Cal nodule	BA4	7.47	0.19	4.11	1.71	0.16	0.18	47.96	0.03	0.25	0.00	37.94	26	24	59	57	5
Cal nodule	BA5	8.68	0.25	4.13	1.80	0.02	0.21	47.70	0.04	0.32	0.00	36.86	32	31	57	81	7
Cal nodule	PI1	7.52	0.23	3.78	1.70	0.04	0.17	48.52	0.03	0.26	0.00	37.74	27	23	68	76	7
Cal nodule	PI2	9.85	0.27	5.05	2.01	0.02	0.21	45.66	0.03	0.37	0.00	36.53	33	23	119	73	7
Cal nodule	PI4	9.41	0.28	4.20	1.79	0.03	0.19	46.91	0.03	0.30	0.00	36.86	30	25	43	84	7
	mean	**8.67**	**0.25**	**4.19**	**1.80**	**0.05**	**0.19**	**47.44**	**0.03**	**0.30**	**0.00**	**37.07**	**30**	**24**	**65**	**76**	**7**
terra rossa	TR1	49.33	1.31	23.27	8.89	0.18	1.02	2.32	0.25	2.10	0.10	11.24	166	96	52	398	42
terra rossa	TR2	50.34	1.41	23.17	8.62	0.20	0.85	2.32	0.19	1.77	0.08	11.04	139	79	56	410	39
terra rossa	TR3	48.90	1.37	22.33	8.58	0.18	0.80	3.69	0.18	1.70	0.08	12.19	132	80	60	411	38
	mean	**49.52**	**1.36**	**22.92**	**8.70**	**0.19**	**0.89**	**2.78**	**0.21**	**1.86**	**0.09**	**11.49**	**146**	**85**	**56**	**406**	**40**

The two samples of unaltered limestone (CA1 and CA2) show a typical calcareous composition in which calcium of calcite can be substituted by strontium.

The thinnest incrustation (CA1C, thickness of 0.5 cm) shows a slight increase in Al_2O_3, Fe_2O_3, SiO_2, Rb, and Zr. The increase of the same elements become more consistent in the thickest incrustation (CA2C, thickness of about 2 cm), in which also Ti, Na, Mn and Y show higher contents (Table 1). The enrichment of these elements is related to the presence of the impure calcite, Fe-kaolinite and (Mn, Ba, Ca) phases (Figure 5a).

The eight samples of calcite nodules have a similar chemical composition, and on average they show a composition like to the thickest incrustation (Table 1). In fact, the mineral phases present in the nodules are comparable with those of the incrustation CA2C. In addition, detrital silicate phases and volcanic lithics, also visible under the optical microscope, suggest the incorporation of external material in both the incrustation growth and the nodule accretion.

The fine-grained portion of *terra rossa* has a significantly different chemical composition showing high contents of SiO_2 (49.52%), Al_2O_3 (22.92%), Na_2O (0.21 wt%), K_2O (1.86 wt%), TiO_2 (1.36%), Fe_2O_3 (8.70%), MgO, Zr and Nb with respect to red incrustations and calcite nodules, whereas the CaO and LOI values decrease significantly (Table 1). The occurrence of goethite, hematite, kaolinite, and heavy minerals such as zircons support these chemical compositions.

The regular increase of TiO_2, Fe_2O_3, Al_2O_3 and alkaline elements from bedrock to *terra rossa* is shown in Figure 7. It is evident how the chemistry of the succession changes from calcareous composition to prevalent fine-grained silicate deposit (Table 1).

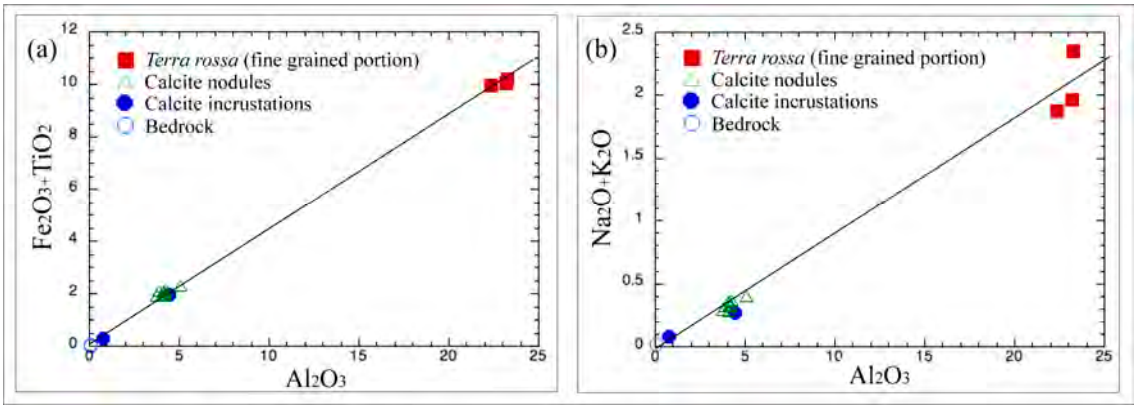

Figure 7. Binary diagrams: (**a**) Al_2O_3 versus (Fe_2O_3 + TiO_2) and (**b**) Al_2O_3 versus (Na_2O + K_2O).

To better constrain the chemical features of karst products, one sample of the thickest incrustation, two samples of nodules and three samples of a fine-grained portion of *terra rossa* were analyzed for other trace elements and REE (Table 2).

On the behavior of Fe_2O_3 and TiO_2, the Ni, V and Cr increase substantially from the red incrustation to the *terra rossa*. Similar behavior is shown by Th, U, and rare earth elements. ∑REE changes from 135 ppm in the thickest incrustation to 303 ppm in fine-grained portion of *terra rossa*, again a nodule contains REE abundances (131 ppm) such as those of the red incrustation, suggesting a strong genetic linkage between the two. In addition to the increase of REE in the fine-grained portion of *terra rossa*, a homogeneous pattern is also observed for these with LREE enrichment (295 ppm), no Ce anomaly (Ce/Ce* = 1.00), negative Eu anomaly (Eu/Eu* = 0.66), regular Sm/Nd ratio (0.21) and slight enrichment of HREE (Figure 8). In contrast, in red incrustation and nodules, a strong negative Ce anomaly (Ce/Ce* = 0.37, mean on three samples) can be observed related to the oxidation state of the Ce and a constant Sm/Nd ratio (0.20) (Figure 8).

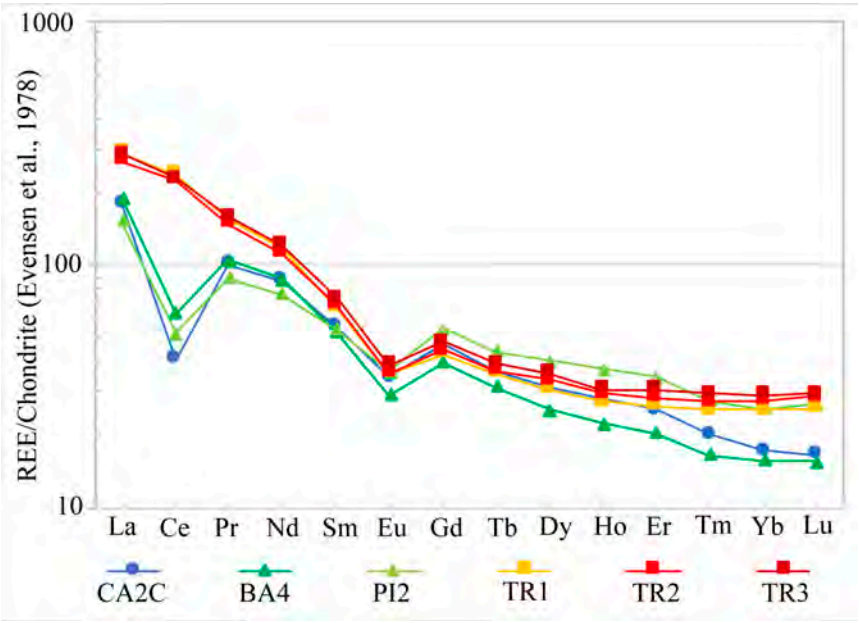

Figure 8. REE patterns normalized to chondrite [40] for selected samples. (CA2C: thickest incrustation; BA4 and PI2: calcite nodules; TR1, TR2, TR2: fine-grained portion of *terra rossa*).

Table 2. Trace elements comprehensive of rare earth elements in selected samples (fusion ICP/MS method).

	Sample	La	Ce	Pr	Nd	Sm	Eu	Gd	Tb	Dy	Ho	Er	Tm	Yb	Lu	∑LREE	∑REE	Eu/Eu*	Ce/Ce*	V	Ni	Cr	Cu	Zn	Ga	Cs	Ba	Hf	Ta	Pb	Th	U
Cal incrust	**CA 2C**	43.7	26.1	9.72	40.8	8.56	2.01	9.59	1.38	7.94	1.59	4.23	0.513	2.85	0.419	128.88	134.67	0.67822	0.27681	57	60	40	20	30	6	1.5	857	0.9	0.27	7	3	0.63
Cal nodule	**BA 4**	46.1	40.2	10.1	41.2	8.14	1.7	8.16	1.19	6.47	1.27	3.38	0.423	2.59	0.394	145.74	150.85	0.63765	0.40754	44	30	50	20	30	5	1.3	173	1.3	0.3	7	3	0.67
Cal nodule	**PI 2**	37.1	33.1	8.49	35.9	8.4	2.1	11.3	1.66	10.3	2.12	5.76	0.715	4.25	0.68	122.99	130.74	0.65892	0.4106	49	30	50	20	50	6	1.6	60	1.6	0.41	8	3.93	0.69
terra rossa	**TR 1**	70.7	151	14.8	54.9	10.3	2.08	8.77	1.34	7.85	1.55	4.39	0.653	4.17	0.653	301.7	309.26	0.66909	1.0233	191	60	170	30	100	23	10.1	420	8.1	2.31	35	21.4	2.82
terra rossa	**TR 2**	65.7	143	14.3	52.7	10.6	2.09	9.09	1.38	8.51	1.67	4.71	0.703	4.59	0.737	286.3	294.42	0.65092	1.0371	202	60	190	30	90	22	7.6	330	8.8	2.15	32	19.2	2.86
terra rossa	**TR 3**	69.4	145	15.2	57.1	11.3	2.26	9.9	1.47	9.17	1.75	5.12	0.762	4.86	0.753	298	306.64	0.65323	0.99121	205	70	200	30	90	23	7.7	325	9	2.31	32	19.2	2.95

5. Discussion

5.1. Terra Rossa and Bauxites in the Apulian Karst

Terra rossa and bauxites characterize the karst landscape of the Murge area [38], and they represent residual deposits related to the multiple exposure phases of the Apulia Carbonate Platform [11,12]. The comparison between geochemical features of the investigated *terra rossa* and the bauxites is relevant for the purpose of the present research study. In particular, the rare earth element contents, and relative patterns, give valuable insight on the provenance of clastic sediments [6].

The collected chemical data from the studied fine-grained portion of terra rossa are different to those from the Cretaceous bauxites cropping out in southern Italy, the latter economically exploited in the last century [41]. The Cretaceous Apulian bauxites from Spinazzola, Otranto, and San Giovanni Rotondo (SGR) sites were studied in detail for both major and trace elements [14,15,18], and they show a strong enrichment in Al_2O_3, FeO, TiO_2 and a wide variability of REE content (Figure 9).

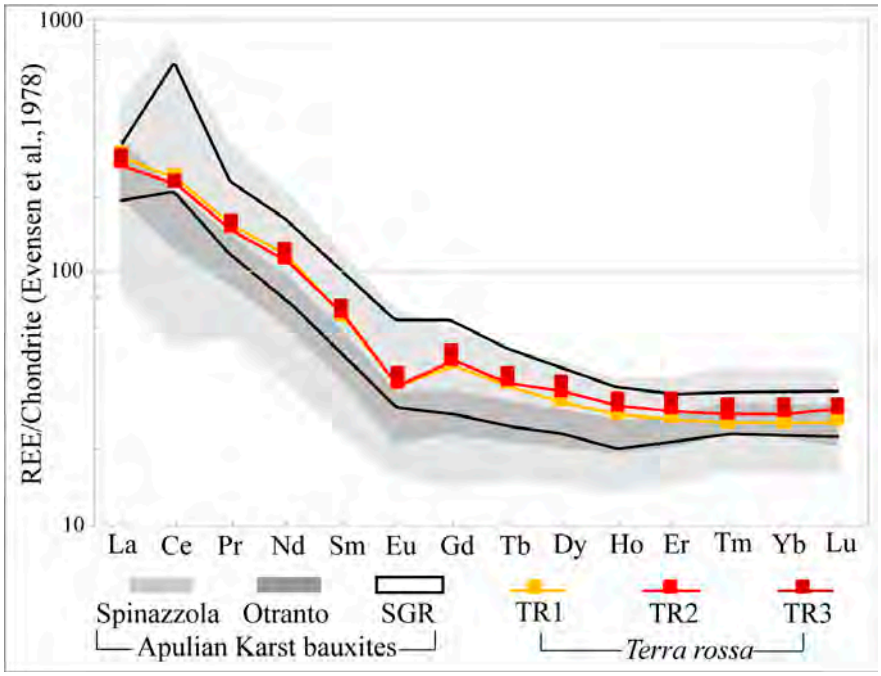

Figure 9. REE patterns normalized to chondrite [40] for studied fine-grained portion of terra rossa (n = 3) compared to literature data for Apulian bauxites [14,15,18].

The comparison between typical Apulian bauxites and the studied fine-grained portion of *terra rossa* shows that the latter is richer in SiO_2 and poorer in Al_2O_3, FeO and TiO_2, whereas the REE contents can be similar in some cases (Figure 9). REE contents from the Spinazzola bauxites are highly variable (∑REE ranging from 152 ppm to 1167 ppm, with negative and positive Ce anomalies), including the contents of the other Apulian bauxites [14,15,18], and also those of the studied fine-grained portion of *terra rossa* (Figure 9).

The similarities in the contents and REE patterns of the Apulian bauxites with the studied *terra rossa*, suggest that the latter may represent an intermediate product leading to the formation of bauxites.

5.2. Genesis of Terra Rossa and Inferences on the Source Material

Two main theories were proposed about the origin of the *terra rossa*: (i) it represents the insoluble *residuum* left by dissolution of limestones [8,9]; (ii) it was produced by the interaction between limestones and allochthonous clastic input, such as alluvial and colluvial sediments, volcanic ash or eolian dust, which may have locally covered the carbonate bedrock [6,7,10]. The first theory has a weakness about the unrealistically large thickness of

limestones to be dissolved to yield significant thickness of *terra rossa*. On the other hand, the second one often neglects the common association of *terra rossa* and karst carbonate rocks [42].

The fine-grained portion of *terra rossa* studied in this work is characterized by high contents of SiO_2, Al_2O_3, Fe_2O_3 (Table 1, Figure 7). It is unquestionable that this strong silicate character requires a considerable supply of allochthonous material providing a silica component. Speculatively, the Quaternary terraced marine deposits (Middle and Upper Pleistocene, Figure 1c) may represent the source of this siliciclastic input. These deposits are described as coastal/transitional mixed carbonate/siliciclastic sediments showing a granulometry varying from sands to clays (e.g., [11,32,43]), characterized by a medium degree of permeability [44].

As a matter of fact, the silicate minerals (quartz, feldspar, zircon) observed in fine-grained *terra rossa*, as well as in the red calcite incrustations and nodules, can represent relicts of these deposits reworked by erosive processes. In addition, the Ti/Cr and Cr/Zr ratios of the fine-grained portion of *terra rossa* around 44 and 0.46 (Table 2), respectively, together with the occurrence of quartz, K-feldspar, zircon and rhyolitic volcanic fragments in the red incrustations and nodules indicate that the allochthonous material was probably acidic in composition comparable with typical clayey deposits.

Therefore, it is our opinion that the simultaneous action of carbonate dissolution and interaction with supplied material, could represent the solution to explain the origin, and the observed thickness, of the studied *terra rossa*. These processes of *terra rossa* formation are represented in the four-step synoptic cartoon of Figure 10, where the interaction between the silicate material and the limestone, accompanied by the dissolution of $CaCO_3$, are contemplated. In particular, the water with CO_2 is enriched with SiO_2, Al, and Fe from the silicate material. At the interface between the silicate material and the underlying limestone, this aqueous solution determines a reaction front, where it is enriched also with Ca, HCO_3^- and CO_3^- released from the dissolution of limestone (Figure 10). A favorable hydrogeological setting characterized by the establishment of a vadose zone has promoted these processes during the formation of the *terra rossa*.

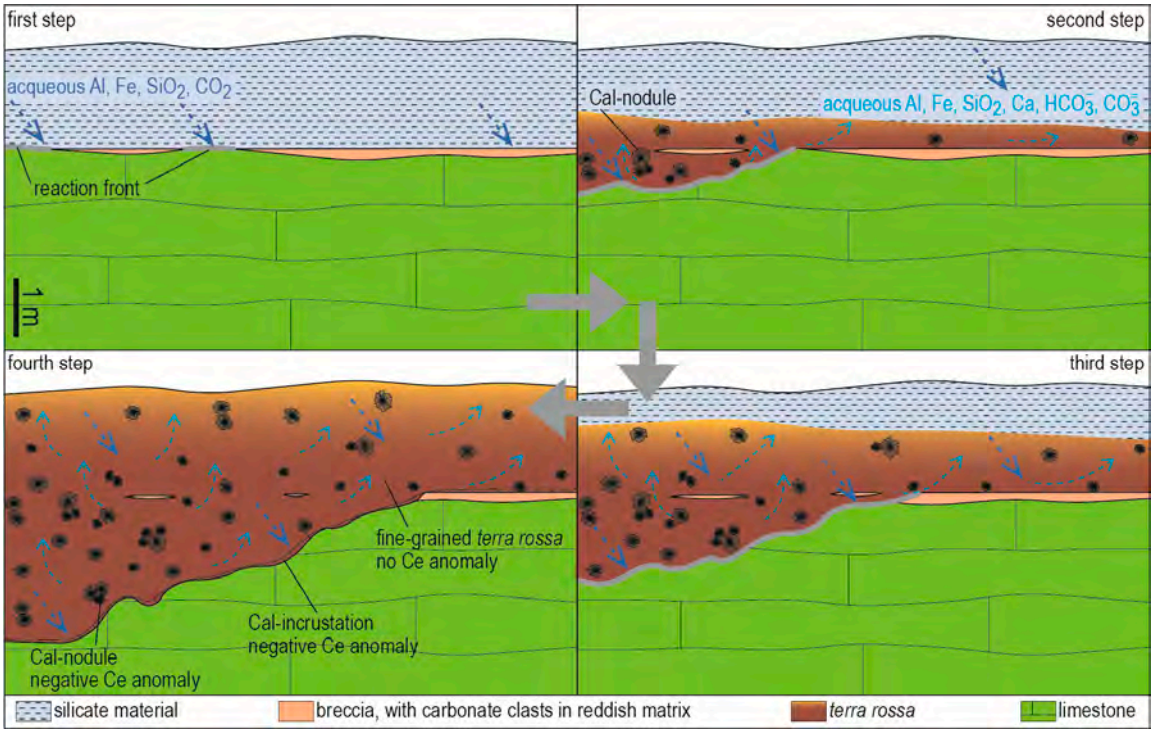

Figure 10. Synoptic cartoon showing four schematic steps for the progressive formation of the *terra rossa* in the study area (see text for further explanations).

According to our results, the studied morphological depression is a typical solution doline (e.g., [45–47]), shaped by interaction processes between limestones and the silicate materials above.

The interaction between limestones and external contributions (such as siliciclastic or volcaniclastic materials) is similarly invoked for the origin of the Cretaceous *terra rossa* and bauxites from Apulia Carbonate Platform, based on geochemical and mineralogical evidence [13–18].

The presence of aqueous solutions with suspended clayey particles and dissolved ions should, together, facilitate the limestones dissolution, with formation of typical authigenic minerals, such as hematite, goethite, kaolinite and anatase, that to a large extent form the fine-grained portion of *terra rossa*. In accordance with [42], the abundance of kaolinite ($Al_2Si_2O_5(OH)_4$) containing even Fe^{3+}, is due to the replacement by pressure of the $CaCO_3$ following the interaction between silicate aqueous solutions and limestones.

The formation of these authigenic minerals occurred together with the development of the red calcite nodules, from an aqueous solution oversaturated in Ca (Figure 10), with SiO_2, Fe and Al impurities (Figures 5 and 6); with a similar process, the impure red calcite incrustations occurred on the limestone at the interface with the *terra rossa* (Figure 10). According to [42], the acidic solutions, generated by dissolution of $CaCO_3$, favored the increase in porosity of the calcareous bedrock, which thus became more and more easily weathered and reactive with the silicate component.

The *terra rossa* represents a kind of silicate distillate whereby Al-rich clay minerals containing LREE are concentrated (Table 2, Figure 8). This is corroborated by the REE fractionation pattern, with $(La/Yb)_N$ ranging from 9.7 to 11.5, the negative Eu anomaly (Eu/Eu* ranges from 0.65 to 0.67) comparable with $(La/Yb)_N$ ratio (9.2–16.4), and the Eu anomaly (Eu/Eu* 0.60–0.70) of Post-Archean Australian Shale [48] (Table 2, Figure 8).

The reinforcement of this idea comes from a comparison of the chemical composition of the fine-grained portion of *terra rossa*, with that of clayey deposits cropping out close to the study site. A chemical comparison with these Turonian clay-rich beds [19] indicates a similar chemical and mineralogical composition: goethite, kaolinite, hematite and anatase as prevalent mineral phases, Al_2O_3 content around 27 wt%, and an LREE fractionated pattern with Eu/Eu* = 0.62 and Sm/Nd = 0.22. [19] suggest for these deposits an origin from both intermediate silicate pyroclastics and minor limestone residuum. This suggestion is consistent with the petrographic features of the red incrustations, nodules, and the fine-grained portion of *terra rossa* at the investigated site.

5.3. Some Remarks on the Cerium Behaviour

Further relevant deductions regarding aqueous solution palaeo-conditions derive from cerium behaviour. Cerium (Ce^{3+}, Ce^{4+}) is generally considered a natural proxy for revealing interaction processes between particles and solutions, and redox reactions [49]. These geochemical features allow carbonate sedimentologists to reconstruct ancient environmental conditions. Ce^{4+} is insoluble and can form the cerianite (CeO_4) in the pH range 5–6 with Eh values between 0.38 V and 0.61 V [50,51]. In contrast, Ce^{3+} is soluble under anoxic conditions and prefers aqueous solutions.

The strong Ce negative anomalies in the red incrustations and the nodules (Ce/Ce* = 0.28 and Ce/Ce* = 0.41, respectively, Table 2, Figure 8) are related to anoxic conditions in which Ce^{3+} is soluble in aqueous solution and moves away from the red incrustations and nodules, whereas the absence of Ce anomalies in the fine-grained portion of *terra rossa* (Figure 9) indicates more oxygenated conditions (Figure 10). In such an environment, LREE, Zn, Cu and Pb also tend to be concentrated, as evidenced by higher contents of these elements in the fine-grained portion of *terra rossa* (Table 2).

The results of the investigations carried out show that the formation of red incrustations and calcite nodules was considerably favored by the interaction with pelite material under wet anoxic conditions in the karst environment on the Mesozoic limestones.

Finally, it would seem that the anoxic conditions during red incrustations and nodules formation are also related to the precipitation of (Mn, Ba, Ca) phases.

6. Conclusions

We performed integrated geological, textural, petrographic, and geochemical analyses of a succession consisting of calcareous substrate, red calcite incrustations, reddish calcite nodules up to *terra rossa* soil with the aim to define the formation processes of this residual deposit.

Starting from the calcareous bedrock, a regular increase of TiO_2, Fe_2O_3, Al_2O_3 and SiO_2 in the red incrustations and calcite nodules can be observed. The mineralogical composition and chemistry of red incrustation and nodules are comparable: fibrous and impure calcite is prevalent together with quartz, (Mn, Ba, Ca) phases, (Al, Si, Mn, Fe, Mg, Ba, Ca) minerals, Fe-kaolinite and anatase; in addition, the REE patterns are comparable, showing negative Ce and Eu anomalies, which suggests that their genesis was similar. In contrast, the fine-grained portion of *terra rossa* has a strong silicate character with SiO_2 values around 49 wt%, Al_2O_3 and Fe_2O_3 contents in average 23 wt% and 8.7 wt%, respectively. This is also rich in LREE, Ni, V, Cr, Zn, Cu, Pb, Th and U with a negative Eu anomaly and no Ce anomaly. The prevalent minerals are hematite, kaolinite, and goethite.

Based on changing Ce anomaly from negative in red incrustation and nodule to no anomaly in fine-grained *terra rossa*, different environmental conditions can be envisaged: an oxygenated environment persists during the accumulation of allochthonous siliciclastic input; anoxic conditions prevail in the underlying levels of the incremental limestone karst, due to percolation of acidic and silicate solutions, producing more or less thick red incrustations, calcite nodules, and clayey *terra rossa*.

These preliminary data indicate that the karst alteration process on limestone was promoted and accelerated by allochthonous siliciclastic material supply and silicate solution circulation between the carbonate bedrock and the overhead pelite materials.

Author Contributions: Conceptualization, F.M., A.F. and V.F.; methodology, F.M., A.F. and V.F.; software, F.M., A.F. and V.F.; validation, F.M., A.F., V.F., M.P., F.T., S.G. and L.S.; investigation and analysis, F.M., A.F., L.S. and V.F.; data curation, F.M., A.F., L.S. and V.F.; data discussion, F.M., A.F., V.F., M.P., F.T., S.G. and L.S.; writing—original draft preparation, F.M., A.F. and V.F.; review, F.M., A.F., V.F., M.P., F.T., S.G. and L.S.; editing, F.M. and V.F.; supervision, F.M.; funding acquisition, F.M., V.F., S.G. and L.S. All authors have read and agreed to the published version of the manuscript.

Funding: This research was funded by Aldo Moro Bari University (Italy) by 2020 Ateneo and Horizon Europe Seeds (S01) grants.

Data Availability Statement: All authors agree to share the research data acquired in this work, and no privacy or ethical restrictions exist.

Acknowledgments: We thank Pasquale Acquafredda, Nicola Mongelli and Mauro Pallara for their assistance during SEM and XRD analyses. Two anonymous reviewers are thanked for their constructive criticism.

Conflicts of Interest: The authors declare no conflict of interest. The funders had no role in the design of the study; in the collection, analyses, or interpretation of data; in the writing of the manuscript, or in the decision to publish the results.

References

1. Williams, P.W. The role of the subcutaneous zone in karst hydrology. *J. Hydrol.* **1983**, *61*, 45–67. [CrossRef]
2. Williams, P.W. The role of the epikarst in karst and cave hydrogeology: A review. *Int. J. Speleol.* **2008**, *37*, 1–10. [CrossRef]
3. White, W.B. Karst hydrology: Recent developments and open questions. *Eng. Geol.* **2002**, *65*, 85–105. [CrossRef]
4. Palmer, A.N. Understanding the hydrology of karst. *Geol. Croat.* **2010**, *63*, 143–148. [CrossRef]
5. Stevanovic, Z. *Karst Aquifers—Characterization and Engineering*; Professional Practice in Earth Science Series; Springer International: Basle, Switzerland, 2015.
6. Durn, G. Terra rossa in the Mediterranean region: Parent materials, composition and origin. *Geol. Croat.* **2003**, *56*, 83–100. [CrossRef]

7. Muhs, D.R.; Budahn, J.; Avila, A.; Skipp, G.; Freeman, J.; Patterson, D. The role of African dust in the formation of Quaternary soils on Mallorca, Spain and implications for the genesis of Red Mediterranean soils. *Quat. Sci. Rev.* **2010**, *29*, 2518–2543. [CrossRef]
8. White, W.B. *Geomorphology and Hydrology of Karst Terrains*; Oxford University Press: New York, NY, USA, 1988; p. 480.
9. Ford, D.C.; Williams, P. *Karst Hydrogeology and Geomorphology*; John Wiley and Sons Inc.: Chichester, UK, 2007.
10. Singer, A. *The Soils of Israel*; Springer: Berlin/Heidelberg, Germany, 2007; p. 306. [CrossRef]
11. Ciaranfi, N.; Pieri, P.; Ricchetti, G. Note alla Carta Geologica delle Murge e del Salento (Puglia centromeridionale). *Mem. Della Soc. Geol. Ital.* **1988**, *41*, 449–460.
12. Spalluto, L.; Pieri, P.; Ricchetti, G. Le facies carbonatiche di piattaforma interna del Promontorio del Gargano: Implicazioni paleoambientali e correlazioni con la coeva successione delle Murge (Italia meridionale, Puglia). *Boll. Soc. Geol. Ital.* **2005**, *124*, 675–690.
13. Yu, W.; Oggiano, G.; Mongelli, G.; Zhou, J.; Buccione, R.; Xu, L.; Mameli, P.; Du, Y. U-Pb detrital zircon ages and Hf isotope from Sardinia and Adria Cretaceous bauxite (Italy): Constraints on the Alpine Tethys paleogeography and tectonic evolution. *Ore Geol. Rev.* **2022**, *153*, 105272. [CrossRef]
14. Mongelli, G.; Boni, M.; Buccione, R.; Sinisi, R. Geochemistry of the Apulian karst bauxites (southern Italy). Chemical fractionation and parental affinities. *Ore Geol. Rev.* **2014**, *63*, 9–21. [CrossRef]
15. Mongelli, G.; Buccione, R.; Gueguen, E.; Langone, A.; Sinisi, R. Geochemistry of the apulian allochthonous kars bauxite, Southern Italy: Distibution of critical elements and constraints on Late Cretaceous Peri-Tethyan palaeogeography. *Ore Geol. Rev.* **2016**, *77*, 246–259. [CrossRef]
16. Mongelli, G.; Boni, M.; Oggiano, G.; Mameli, P.; Sinisi, R.; Buccione, R.; Mondillo, N. Critical metals distribution in Tethyan karst bauxite: The cretaceous Italian ores. *Ore Geol. Rev.* **2017**, *86*, 526–536. [CrossRef]
17. Buccione, R.; Mongelli, G.; Sinisi, R.; Boni, M. Relationship between geometric parameters and compositional data: A new approach to karst bauxites exploration. *J. Geochem. Explor.* **2016**, *169*, 192–201. [CrossRef]
18. Sinisi, R. Mineralogical and geochemical features of Cretaceous bauxite from San Giovanni Rotondo (Apulia, Southern Italy): A provenance tool. *Minerals* **2018**, *8*, 567. [CrossRef]
19. Morelli, F.; Cullers, R.L.; Laviano, R.; Mongelli, G. Geochemistry and palaeoenvironmental significance of Upper Cretaceous clay-rich beds from the Peri-Adriatic Apulia Carbonate Platform, southern Italy. *Period. Di Mineral.* **2000**, *69*, 165–183.
20. Moresi, M.; Mongelli, G. The relation between the terra rossa and the carbonate-free residue of the underlying limestones and dolostones in Apulia, Italy. *Clay Miner.* **1988**, *23*, 439–446. [CrossRef]
21. Vingiani, S.; Di Iorio, E.; Colombo, C.; Terribile, F. Integrated study of red Mediterranean soils from southern Italy. *Catena* **2018**, *168*, 129–140. [CrossRef]
22. Mastronuzzi, G.; Valletta, S.; Damiani, A.; Fiore, A.; Francescangeli, R.; Giandonato, P.B.; Iurilli, V.; Sabato, L. *Geositi Della Puglia. Ricognizione e Verifica Dei Geositi e Delle Emergenze Geologiche Della Regione Puglia*; Graphic Concept Lab: Bari, Italy, 2015; p. 394.
23. Alfonso, G.; Beccarisi, L.; Pieri, V.; Frassanito, A.; Belmonte, G. Using crustaceans to identify different pond types. A case study from the Alta Murgia National Park, Apulia (South-eastern Italy). *Hydrobiologia* **2016**, *782*, 53–69. [CrossRef]
24. Festa, V.; Teofilo, G.; Tropeano, M.; Sabato, L.; Spalluto, L. New insights on diapirism in the Adriatic Sea: The Tremiti salt structure (Apulia offshore, southeastern Italy). *Terra Nova* **2014**, *26*, 169–178. [CrossRef]
25. Tropeano, M.; Pieri, P.; Moretti, M.; Festa, V.; Calcagnile, G.; Del Gaudio, V.; Pierri, P. Quaternary tectonics and seismotectonic features of the Murge area (Apulian foreland, SE Italy)/Tettonica quaternaria ed elementi di sismotettonica nell'area delle Murge (Avampaese Apulo). *Alp. Maditerranean Quat.* **1997**, *10*, 543–548.
26. Festa, V. Cretaceous structural features of the Murge area (Apulian Foreland, Southern Italy). *Ecol. Geol. Helv.* **2003**, *96*, 11–22. [CrossRef]
27. Selli, R. Il Paleogene nel quadro della geologia dell'Italia meridionale. *Mem. Soc. Geol. It* **1962**, *3*, 737–790.
28. Ricchetti, G.; Ciaranfi, N.; Luperto Sinni, E.; Mongelli, F.; Pieri, P. Geodinamica ed evoluzione sedimentaria e tettonica dell'avampaese apulo. *Mem. Soc. Geol. It.* **1988**, *41*, 57–82.
29. Sauro, U. A polygonal karst in the Alte Murge (Puglia, Southern Italy). *Z. Geomorph.* **1991**, *35*, 207–223. [CrossRef]
30. Parise, M. Surface and subsurface karst geomorphology in the Murge (Apulia, southern Italy). *Acta Carsologica* **2011**, *40*, 79–93. [CrossRef]
31. Iannone, A.; Pieri, P. Neotectonic characteristics of the Murge area/Caratteri neotettonici delle Murge. *Geol. Appl. E Idrogeol.* **1982**, *17*, 147–159.
32. Spalluto, L.; Pieri, P.; Sabato, L.; Tropeano, M. Nuovi dati stratigrafici e cartografici delle unità quaternarie del Foglio 438 "BARI" (Puglia-Italia meridionale). *Alp. Mediterr. Quat.* **2010**, *23*, 3–14.
33. Festa, V.; Fiore, A.; Parise, M.; Siniscalchi, A. Sinkhole evolution in the Apulian karst of southern Italy: A case study, with some considerations on sinkhole hazards. *J. Cave Karst Stud.* **2012**, *74*, 137–147. [CrossRef]
34. Pepe, M.; Parise, M. Structural control on development of karst landscape in the Salento Peninsula (Apulia, SE Italy). *Acta Carsologica* **2014**, *43*, 101–114. [CrossRef]
35. Acquafredda, P.; Muntoni, I.M.; Pallara, M. Reassessment of WD-XRF method for obsidian provenance shareable databases. *Quat. Int.* **2018**, *468*, 169–178. [CrossRef]
36. Spalluto, L.; Caffau, M. Stratigraphy of the mid-Cretaceous shallow-water limestones of the Apulia Carbonate Platform (Murge, Apulia, southern Italy). *Ital. J. Geosc.* **2010**, *129*, 335–352. [CrossRef]

37. Spalluto, L. Facies evolution and sequence chronostratigraphy of a mid-Cretaceous shallow-water carbonate succession of the Apulia Carbonate Platform from the Northern Murge area (Apulia, southern Italy). *Facies* **2012**, *58*, 17–36. [CrossRef]
38. Chiocchini, M.; Farinacci, A.; Mancinelli, A.; Molinari, V.; Potetti, M. Biostratigrafia a foraminiferi, dasicladali e calpionelle delle successioni carbonatihce mesozoiche dell'Appennino centrale (Italia). *Studi Geol. Camerti. Biostratigrafia Dell'italia Cent.* **1995**, *1994*, 9–12.
39. Checconi, A.; Rettori, R.; Spalluto, L. Biostratigrafia a foraminiferi del Cretaceo Superiore della successione di Parco Priore (Calcare di Altamura, Piattaforma Apula, Italia Meridionale). *Ann. Dell'univ. Di Ferrara Mus. Sci. Nat.* **2008**, *4*, 1–11.
40. Evensen, N.M.; Hamilton, P.J.; O'nions, R.K. Rare-earth abundances in chondritic meteorites. *Geochim. Et Cosmochim. Acta* **1978**, *42*, 1199–1212. [CrossRef]
41. Mondillo, N.; Balassone, G.; Boni, M.; Rollinson, G. Karst bauxites in the Campania Apennines (southern Italy): A new approach. *Period. Di Mineral.* **2011**, *80*, 407–432.
42. Merino, E.; Banerjee, A. Terra rossa genesis, implications for karst, and eolian dust: A geodynamic thread. *J. Geol.* **2008**, *116*, 62–75. [CrossRef]
43. Dell'Anna, L.; De Marco, A.; Ricchetti, G.; Di Pierro, M. Ricerche geologiche e mineralogiche sulle "Calcareniti di Monte Castiglione". *Boll. Soc. Geol. It* **1978**, *97*, 451–474.
44. Allocca, V.; Celico, F.; Celico, P.; De Vita, P.; Fabbrocino, S.; Mattia, C.; Monacelli, G.; Musilli, I.; Piscopo, V.; Scalise, A.R.; et al. *Carta Idrogeologica Dell'italia Meridionale*; Istituto Poligrafico e Zecca Dello Stato: Roma, Italia, 2007.
45. Gutierrez, F.; Parise, M.; De Waele, J.; Jourde, H. A review on natural and human-induced geohazards and impacts in karst. *Earth Sci. Rev.* **2014**, *138*, 61–88. [CrossRef]
46. Parise, M. Sinkholes. In *Encyclopedia of Caves*, 3rd ed.; White, W.B., Culver, D.C., Pipan, T., Eds.; Academic Press, Elsevier: Cambridge, MA, USA, 2019; pp. 934–942. ISBN 978-0-12-814124-3.
47. Parise, M. Sinkholes, Subsidence and Related Mass Movements. In *Treatise on Geomorphology*; Shroder, J.J.F., Ed.; Academic Press, Elsevier: Cambridge, MA, USA, 2022; Volume 5, pp. 200–220.
48. Taylor, S.R.; McLennan, S.M. *The Continental Crust: Its Composition and Evolution*; Blackwell Scientific Publications: Oxford, UK, 1985; p. 312.
49. Özyurt, M.; Kırmacı, M.Z.; Al-Aasm, I.; Hollis, C.; Taslı, K.; Kandemir, R. REE characteristics of Lower Cretaceous Limestone Succession in Gümüşhane, NE Turkey: Implications for Ocean Paleoredox conditions and diagenetic alteration. *Minerals* **2020**, *10*, 683. [CrossRef]
50. Braun, J.J.; Pagel, M.; Muller, J.P.; Bilong, P.; Michard, A.; Guillet, B. Cerium anomalies in lateritic profiles. *Geochim. Et Cosmochim. Acta* **1990**, *54*, 781–795. [CrossRef]
51. Mongelli, G. Ce-anomalies in the textural components of Upper Cretaceous karst bauxites from the Apulian carbonate platform (southern Italy). *Chem. Geol.* **1997**, *140*, 69–79. [CrossRef]